A&A 379, 54–71 (2001)
DOI: 10.1051/0004-6361:20011275

Astronomy & Astrophysics

$BVRI$ surface photometry of (S+S) binary galaxies⋆

I. The data⋆⋆

H. M. Hernández-Toledo[1] and I. Puerari[2]

[1] Instituto de Astronomía – UNAM – Apartado Postal 70-264, 04510 México DF, México
[2] Instituto Nacional de Astrofísica, Optica y Electrónica, Calle Luis Enrique Erro 1, 72840 Tonantzintla, Puebla, México
e-mail: puerari@inaoep.mx

Received 28 February 2001 / Accepted 21 August 2001

Abstract. We present multicolour broad band ($BVRI$) photometry for a sample of 33 spiral-spiral (S+S) binary galaxies drawn from the Karachentsev Catalogue of Isolated Pairs of Galaxies (KPG). The data is part of a joint observational programme devoted to systematic photometric study of one of the most complete and homogeneous pair samples available in the literature. We present azimuthally averaged colour and surface brightness profiles, colour index $(B-I)$ maps, B band and sharp/filtered B band images as well as integrated magnitudes, magnitudes at different circular apertures and integrated colours for each pair. Internal and external data comparisons show consistency within the estimated errors. Two thirds of the sample have total aperture parameters homogeneously derived for the first time. After reevaluating morphology for all the pairs, we find a change in Hubble type for 24 galaxies compared to the original POSS classifications. More than half of our pairs show morphological concordance which could explain, in part, the strong correlation in the $(B-V)$ colour indices (Holmberg Effect) between pair components. We find a tendency for barred galaxies to show grand design morphologies and flat colour profiles. The measurements will be used in a series of forthcoming papers where we try to identify and isolate the main structural and photometric properties of disk galaxies at different stages of interaction.

Key words. galaxies: spiral – galaxies: structure – galaxies: photometry – galaxies: interactions – galaxies: fundamental parameters – galaxies: kinematics and dynamics

1. Introduction

Two-dimensional broad-band photometry has been systematically applied to the study of binary galaxy structure and dynamics, only in the past two decades. The mid to late 70's saw an astronomical debate that led to the recognition that gravitational interaction is an important factor in galactic evolution affecting directly properties such as size, morphological type, luminosity, star formation rate, and mass distribution (Sulentic 1976; Larson & Tinsley 1978; Stocke 1978). According to current popular models of galaxy formation, galaxies are assembled through a hierarchical process of mass aggregation, dominated either by mergers (Kauffmann et al. 1993; Baugh et al. 1996) or by gas accretion (Avila-Reese et al. 1998; Avila-Reese & Firmani 2000). In the light of these models, the influence of environment factors and interaction phenomena in the shaping and star formation of the disks is natural, at least for a fraction of the present-day galaxy population. Examples are galaxy harassment in clusters (Moore et al. 1996), tidal stirring of dwarf irregulars near giant galaxies (Mayer et al. 2001), tidally induced star formation (Lacey & Silk 1991; Kauffmann et al. 2001). See also Dultzin-Hacyan (1997) for a non-biased review.

For binary galaxies, current ideas suggest that most physical pairs are morphologically concordant, that is, with components showing similar initial star formation and angular momentum properties. Evidence in favour of

Send offprint requests to: H. Hernández-Toledo,
e-mail: hector@astroscu.unam.mx

⋆ Table A.1 is only available in electronic form at the CDS via anonymous ftp cdsarc.u-strasbg.fr (130.79.128.5) or via http://cdsweb.u-strasbg.fr/cgi-bin/qcat?J/A+A/379/54 and Tables 2–4 are also available in electronic form at the CDS. Full Fig. 5 is only available in electronic form at the http://www.edpsciences.org

⋆⋆ Based on data obtained at the 2.1 m telescope of the Observatorio Guillermo Haro at Cananea, Sonora, México, operated by the Instituto Nacional de Astrofísica, Optica y Electrónica.

these ideas come from the colour correlations (Holmberg effect) observed for components of pairs, although very few photometric data supporting this correlation exists at present. The large number of (S+S) pairs in The Catalogue of Isolated Pairs of Galaxies in the Northern Hemisphere (KPG, Karachentsev 1972) means that for a flux-limited sample ($m_{zw} = 15.7$), almost six out of every ten pairs are of the (S+S) type, suggesting that a considerable number of them must be physical binaries.

Redshift information, available for the whole (S+S) sample, suggests that most are likely to be physically proximate. Digital Sky Survey images show that most have visible signs of disturbance; bridges, tails, common envelopes and distortions that are regarded as evidence for gravitational interaction. In addition, statistical studies indicate that a high fraction ($\sim$65%) show an enhancement in the optical and FIR emission (Xu & Sulentic 1991; Hernández-Toledo et al. 1999). This enhancement is interpreted as a by-product of interaction-induced star formation activity in physical binaries.

One of the most important lessons that emerges from statistical studies of interacting galaxies is that if we want to have a better understanding of the connection between interactions, photometric structural parameters and optical morphology, it is necessary to obtain accurate photometry for complete and homogeneous interacting galaxy samples. The results can then be interpreted by applying similar methods to well-matched comparison samples (isolated, presumably undisturbed galaxies). Some efforts in this direction are Bergvall & Johansson (1995), Reduzzi & Rampazzo (1996), Márquez & Moles (1996), Laurikainen et al. (1998), Jansen et al. (2000), Márquez & Moles (1999), and de Jong & van der Kruit (1994).

Our main goal is to obtain an homogeneous set of broad-band observations for most (if not all) of the (S+S) pairs in the Karachentsev Catalogue. The relative simplicity, compared to groups and clusters along with the size, brightness limit and morphological diversity, offer us a unique opportunity to realize accurate photometric observations for a statistically significant number of pairs where a less confused interpretation of the photometric properties of disk galaxies at different stages of interactions (and its relationship to optical morphology) is possible.

We present in this first paper of a series, our photometric data with emphasis on the morphological properties in a subset of 33 (S+S) pairs. The structure of the paper is as follows. Section 2 summarizes some limitations and biases in the (S+S) sample which are relevant to our photometric study. Section 3 presents the observations, reduction techniques and a comparison of our estimated total magnitudes against those in the literature. A discussion on the related errors is also included. Section 4 shows a discussion based on the estimated colour indices, observed optical morphologies and (colour and surface brightness) profiles for each component galaxy. The systematics of morphological distortions induced by the interactions are commented in the light of current models. Section 5 is a summary of the conclusions achieved. Finally, an Appendix is devoted to the presentation of magnitudes at three different concentric circular apertures.

2. Sample and observations

Through the main optical observatories in México (Observatorio Astronómico Nacional at San Pedro Mártir in Baja California and Observatorio Astrofísico Guillermo Haro in Cananea) we have started a joint observational programme devoted to obtain uniform photometric data for one of the most complete and homogeneous pair samples currently available. The sample of disk-disk (S+S) pairs amounts to more than 300 pairs from a total of 602 pairs in the KPG catalogue. The observations were begun since January 1999. The CCD $BVRI$ images reported here (in the Cousins system) were obtained with a LFOSC detector attached to the 2.1 m telescope, at Observatorio Guillermo Haro, Cananea, Sonora, México, covering an area of about $6' \times 4'$, with a scale of $1''$/pixel.

Since our goal is to observe all or most of the KPG (S+S) sample, we have applied no special strategy in selecting the current subset of 33 (S+S) pairs. Available observing time and weather conditions were the main factors limiting the number of observed pairs. This will be the observational strategy for the next reports up to the point where most of the (S+S) sample is observed. The selection criteria and statistical properties for the (S+S) sample that are most relevant to the present and further photometric analysis are stated here.

2.1. Statistical properties of the (S+S) sample

The isolated (S+S) pairs in the KPG sample were selected from a visual search of the Palomar Sky Survey. The catalogue samples the sky north of $\delta \geq -3°$. The vast majority of objects are found in high Galactic latitude regions ($b \geq 20°$) and as a sample, they are reasonably complete ($\sim$90%) in the magnitude range $13.5 \leq m_{zw} \leq 15.7$. All galaxies in the (S+S) sample have measured redshifts. We next summarize possible limitations and sources of bias (mainly due to the optical selection criteria) that may affect the interpretation of the photometric analysis.

(1) Although the projected physical separation ($H_0 = 75$ km s^{-1} Mpc^{-1}) for the whole (S+S) sample is small ($< x > = 42.1$ kpc), there is still a source of contamination from accordant redshift optical pairs. This is a difficult source to evaluate because most such optical pairs are members of loose group structures with magnitude and redshift properties completely within the domain of expectation for physical binary systems. Our photometric study, however, is most useful for solving the problem if we observe as much as possible the fraction of the (S+S) sample that shows direct/indirect signs of interactions. That is, by observing the most probable physical pairs, on an individual basis;

(2) The (S+S) sample will reject highly evolved pairs such as mergers in the final stages of coalescence.

This stems from the selection requirement that the galaxies have a discernible diameter. This excludes, for example, ultra-luminous infrared galaxies (ULIRGs) from our photometric study of (S+S) pairs;

(3) The maximum size ratio between components (from the basic selection criteria) is $a_2/a_1 \sim 8$. This means that the (S+S) sample favours magnitude and thus size concordance, biasing this sample against hierarchical binaries. However, an important difference in visual apparent magnitudes between member pairs ($\Delta m \sim 3^{\rm m}$) can be found;

(4) (S+S) pairs with the faintest apparent magnitudes must have smaller apparent separations in order to survive the isolation criterion and enter the Karachentsev catalogue. This means that apparently close pairs are biased towards physically close binaries – pairs near pericenter (van Moorsel 1982), or with smaller mean physical separations. By selecting the brightest (S+S) pairs, we therefore sample a wider range of physical separations in our photometric study;

(5) The (S+S) pairs were selected whith a strong isolation criteria. Thus, we expect that only intrinsic properties of the individual galaxies and the effects of their mutual interactions should affect the observed morphological and photometrical properties.

3. Observations and data reduction

A journal of the first set of the photometric observations is given in Table 1. Column (1) gives the original catalogued number, Cols. (2)–(9) give the number of frames per filter, the integration time (in seconds) and seeing conditions (in arcsec).

Table 2 reports some relevant information for the observed pairs coming from the literature. Column (1) is the KPG catalogued number, Col. (2) reports other identifications, Col. (3) the apparent B magnitude from the Nasa Extragalactic Database (NED), Col. (4) the linear separation (in kpc), Col. (5) the radial velocity in km s^{-1} from NED, and finally, Col. (6) gives the major axis diameter (at $\mu_B = 25$) for each component galaxy (in kpc).

Images were debiased, trimmed, and flat-fielded using standard IRAF[1] procedures. First, the bias level of the CCD was subtracted from all exposures. A run of 5–10 bias images was obtained per night, and these were combined into a single bias frame which was then applied to the object frames. The images were flat-fielded using sky flats taken in each filter at the beginning and/or at the end of each night.

Photometric calibration was achieved by nightly observations of standard stars of known magnitudes from the "Dipper Asterism" M 67 star cluster (Chevalier & Ilovaisky 1991). A total of 29 standard stars with a colour range $-0.1 \leq (B-V) \leq 1.4$ and a similar range in $(V-I)$ were observed. The principal extinction coefficients in B, V, R and I as well as the colour terms were calculated according to the following equations:

$$B - b = \alpha_B + \beta_B (b-v)_0$$
$$V - v = \alpha_V + \beta_V (b-v)_0$$
$$R - r = \alpha_R + \beta_R (v-r)_0$$
$$I - i = \alpha_I + \beta_I (v-r)_0$$

where B, V, R and I are the standard magnitudes, b, v, r and i are the instrumental (and airmass-corrected) magnitudes. α and β are the transformation coefficients for each filter.

In a first iteration, a constant value associated with the sky background was subtracted using an interactive procedure that allows the user to select regions on the frame free of galaxies and bright stars. However, occasionally, at the end of the reduction procedure, we still had images with a noticeable gradient in the sky background. For these images, a fifth-order polynomial was fitted and subtracted from the entire frame. After this processing, the sky background is usually flat to a level $\sim$1$-$2%. Errors in determining the sky background, are, in fact, probably the dominant source of error in the estimation of the colour and surface brightness profiles. For this reason, we decided to apply this polynomial correction to all the images in this work.

The most energetic cosmic-ray events were automatically masked using the COSMICRAYS task and field stars were removed using the IMEDIT task when necessary. Within the galaxy itself, care was taken to identify superimposed stars. A final step in the basic reduction involved registration of all available frames for each galaxy and in each filter to within $\pm$0.1 pixel. This step was performed by measuring centroids for foreground stars on the images and then performing geometric transformations using GEOMAP and GEOTRAN tasks in IRAF.

Elliptical surface brightness contours were fitted using the STSDAS package ISOPHOTE. An initial starting guess for the ellipse-fitting routine was provided interactively by estimating points that represent the ends of the major and minor axis at an isophotal level of relatively high signal-to-noise ratio. Since we are interested on the mean global properties of these profiles and not in their detailed structure, we report azimuthally averaged profiles for spirals by fitting ellipses with a fixed position angle and ellipticity previously determined on the external isophotes of each galaxy. A more detailed analysis and interpretation will be presented in a forthcoming paper (Hernández-Toledo & Puerari, in preparation).

3.1. Errors

Total magnitudes can be calculated by analytically extrapolating a fitting of a disk beyond the outermost isophote

[1] The IRAF package is written and supported by the IRAF programming group at the National Optical Astronomy Observatories (NOAO) in Tucson, Arizona. NOAO is operated by the Association of Universities for Research in Astronomy (AURA), Inc. under cooperative agreement with the National Science Foundation (NSF).

Table 1. Journal of observations. The number of frames per filter, the integration time (in seconds), and the mean *FWHM* for each observation (in arcsec) are given.

Galaxy pair	B	$< B >_{FWHM}$	V	$< V >_{FWHM}$	R	$< R >_{FWHM}$	I	$< I >_{FWHM}$
KPG64	2×1200	2.4	3×180	2.3	5×90	2.6	5×90	3.1
KPG68	1×1200	2.3	5×180	2.5	10×60	2.3	5×120	2.8
KPG75	1×1800	2.1	2×600	2.2	3×240	2.1	3×180	2.7
KPG88	1×1800	2.4	1×1800	2.5	1×1200	2.6	1×900	3.3
KPG98	1×1800	2.6	1×900	2.5	2×300	3.1	2×300	3.1
KPG102	1×1800	2.1	1×1200	2.4	1×600	2.4	1×600	2.6
KPG103	1×1800	2.7	1×600	2.5	1×300	2.5	1×300	2.8
KPG108	1×1800	2.5	1×1200	2.5	1×600	2.2	1×300	2.4
KPG112	1×1800	2.5	3×180	2.3	5×60	2.2	5×60	2.8
KPG125	1×1800	2.6	1×1200	2.9	2×300	3.2	2×300	3.6
KPG136	1×1800	2.7	2×900	2.5	1×600	2.3	2×300	2.9
KPG141	1×1800	2.4	1×1200	2.3	1×600	2.2	1×600	2.5
KPG150	1×1800	2.7	2×600	2.4	2×300	2.4	3×180	2.7
KPG151	1×1800	2.4	1×1200	2.6	1×900	2.2	1×600	3.3
KPG156	1×1800	2.6	1×1200	2.6	1×600	2.9	1×600	3.6
KPG159	1×1800	3.6	1×600	3.4	1×600	3.2	1×300	3.5
KPG160	1×1800	2.5	2×600	2.1	3×240	2.3	3×240	2.8
KPG168	1×1200	3.1	2×300	2.9	3×120	2.9	3×120	3.5
KPG195	1×1200	3.0	2×300	3.2	5×90	2.6	5×90	2.5
KPG211	1×1800	2.7	1×600	2.5	2×240	3.0	3×180	3.7
KPG216	1×1800	2.9	1×1200	2.7	1×600	2.3	1×600	2.4
KPG249	1×1800	3.0	1×600	3.3	1×300	3.5	1×300	3.4
KPG295	1×1800	3.0	2×600	3.2	5×150	3.1	5×120	2.9
KPG302	1×1200	2.3	3×300	2.3	5×180	2.2	6×120	2.7
KPG313	1×1800	3.3	1×600	3.2	3×180	3.1	3×120	2.6
KPG332	1×1800	2.9	1×1200	2.9	2×300	2.5	2×240	2.6
KPG347	1×900	2.8	1×600	3.0	3×180	2.5	3×120	2.6
KPG389	1×1800	3.5	1×1200	3.6	2×600	3.2	2×300	2.6
KPG396	1×1800	2.4	1×1200	2.7	1×900	2.5	1×900	2.7
KPG404	1×900	2.7	2×300	2.9	5×150	3.1	5×120	2.4
KPG426	1×1800	2.9	1×600	3.1	2×300	3.2	3×180	3.0
KPG440	1×1200	2.4	1×900	3.0	2×300	2.8	2×240	2.6
KPG455	1×1800	2.3	1×600	2.5	3×180	2.6	3×180	3.1

to infinity. However, disk fitting is notoriously fraught with uncertainty (cf. Knapen & van der Kruit 1991). Alternatively, we estimate in this work a total magnitude computed from polygonal apertures chosen interactively to assure that they are large enough to contain the whole galaxy and still small enough to limit the errors due to the sky error and light contamination from a neighbor galaxy. This is achieved in each band by using polygonal apertures with and without the the sky background removed within POLYPHOT routines in IRAF. In an Appendix, we are also reporting total magnitudes at three different circular apertures by using the PHOT routines in IRAF. Foreground stars within the aperture were removed interactively. In some cases, the separation of the galaxies allowed us to model the light distribution in each galaxy and then to try an iterative subtraction as reported in Junqueira et al. (1998). In cases where this procedure was not possible, our estimations must be taken with care. See Table 3 and comments on individual objects.

An estimation of the errors in our photometry involves two parts: 1) the procedures to obtain instrumental magnitudes and 2) the uncertainty when such instrumental magnitudes are transformed to the standard system. For 1), notice that the magnitudes produced at the output of the IRAf routines (QPHOT, PHOT and POLYPHOT) have a small error that is internal for those procedures. Since we also have applied extinction corrections to the instrumental magnitudes in this step, our estimation of the errors are mainly concerned with these corrections and the estimation of the airmass. After a least square fitting, the associated errors to the slope for each principal extinction coefficient are; $\delta(k_B) \sim 0.038$, $\delta(k_V) \sim 0.035$, $\delta(k_R) \sim 0.020$ and $\delta(k_I) \sim 0.020$. An additional error $\delta(\text{airmass}) \sim 0.005$ from the airmass routines in IRAF was also considered.

For 2), the zero point and first order colour terms are the most important to consider. After transforming to the standard system, by adopting our best-fit coefficients, the formal errors from the assumed relations for α were 0.05, 0.04, 0.04 and 0.04 in B, V, R and I and 0.04, 0.03, 0.03 and 0.04 for β. To estimate the total error in each band, it is necessary to use the transformation equations and then propagate the errors. Total typical uncertainties are 0.15, 0.14, 0.15 and 0.14 in B, V, R and I bands, respectively.

Table 2. General data for the observed galaxies.

KPG Number	Identif.	B mag	x_{12} (kpc)	$V_{\rm Rad}$ (km s^{-1})	A_{25} (kpc)
KPG64A	UGC 01810	13.42(p)	39.5	7563	55.8
KPG64B	UGC 01813	15.08(p)		7335	27.4
KPG68A	NGC 0935	13.63(p)	17.4	4142	29.3
KPG68B	IC 1801	14.56(p)		4023	19.3
KPG75A	UGC 02222	14.56(p)	21.5	4913	32.0
KPG75B	UGC 02225	15.21(p)		4965	18.6
KPG88A	UGC 02627	14.89(a)	32.7	4224	30.8
KPG88B	UGC 02629	15.28(p)		4128	15.1
KPG98A	UGC 02954	15.23(p)	41.2	5306	17.4
KPG98B	MRK 1081	15.15(p)		5345	16.0
KPG102A	CGCG 393-070	15.50(p)	34.4	10 778	21.0
KPG102B	UGC 03136	15.00(p)		10 674	34.8
KPG103A	CGCG 420-003	15.70(p)	55.2	8313	20.3
KPG103B	UGC 03179	14.46(p)		8337	28.4
KPG108A	UGC 03405	15.32(p)	33.9	3738	20.1
KPG108B	UGC 03410	14.99(p)		3921	29.8
KPG112A	UGC 03445	14.25(p)	9.7	3119	21.3
KPG112B	UGC 03446	13.86(p)		3116	21.2
KPG125A	NGC 2341	13.84(a)	50.9	5227	24.9
KPG125B	NGC 2342	13.10(a)		5276	29.1
KPG136A	CGCG 086-028	14.80(p)	37.8	9907	31.1
KPG136B	CGCG 086-029	15.00(p)		9813	32.1
KPG141A	UGC 04005	14.60(p)	89.8	5044	31.8
KPG141B	CGCG 030-014	14.80(p)		4896	14.4
KPG150A	NGC 2486	14.16(a)	99.3	4649	29.5
KPG150B	NGC 2487	13.23(a)		4841	45.6
KPG151A	UGC 04133	16.00(p)	32.5	9130	50.5
KPG151B	UGC 04134	15.37(p)		8968	32.6
KPG156A	NGC 2535	13.31(a)	27.7	4097	30.9
KPG156B	NGC 2536	14.70(a)		4142	17.0
KPG159A	CGCG 088-052	15.60(p)	26.0	5232	9.9
KPG159B	UGC 04286	14.32(p)		5143	19.9
KPG160A	NGC 2544	13.80(a)	17.4	2828	16.0
KPG160B	CGCG 331-037	15.50(p)		3589	11.0
KPG168A	NGC 2648	12.74(p)	17.6	2060	23.1
KPG168B	CGCG 060-036	15.40(p)		2115	9.2
KPG195A	NGC 2798	13.04(a)	11.5	1726	16.3
KPG195B	NGC 2799	14.32(p)		1865	11.3
KPG211A	NGC 2959	13.65(p)	26.8	4429	29.3
KPG211B	NGC 2961	15.52(p)		4501	12.2
KPG216A	NGC 3018	14.13(p)	17.8	1863	6.45
KPG216B	NGC 3023	13.50(p)		1879	14.7
KPG249A	NGC 3395	12.40(a)	8.8	1625	10.5
KPG249B	NGC 3396	12.63(p)		1625	12.3
KPG295A	NGC 3786	*13.24(p)	14.9	2678	19.2
KPG295B	NGC 3788	13.46(p)		2699	13.9
KPG302A	NGC 3893	11.16(s)	13.9	977	17.1
KPG302B	NGC 3896	13.89(p)		980	5.9
KPG313A	IC 0749	12.92(s)	10.9	784	7.5
KPG313B	IC 0750	12.94(s)		701	9.1
KPG332A	NGC 4298	12.04(s)	9.5	1135	10.3
KPG332B	NGC 4302	12.50(s)		1149	13.0
KPG347A	NGC 4567	12.06(s)	10.8	2274	20.2
KPG347B	NGC 4568	11.68(s)		2255	29.3
KPG389A	NGC 5257	*13.50(p)	36.6	6798	39.0
KPG389B	NGC 5258	*13.49(p)		6757	37.8
KPG396A	UGC 08713	15.25(p)	28.6	4956	24.3
KPG396B	UGC 08715	14.50(p)		4517	22.7

Table 2. continued.

KPG Number	Identif.	B mag	x_{12} (kpc)	$V_{\rm Rad}$ (km s^{-1})	A_{25} (kpc)
KPG404A	NGC 5394	13.70(a)	26.2	3472	22.8
KPG404B	NGC 5395	12.10(a)		3491	34.1
KPG426A	UGC 09376	14.70(p)	26.8	7676	40.6
KPG426B	CGCG 220-030	14.89(p)		7764	46.8
KPG440A	NGC 5774	12.74(s)	27.2	1567	20.9
KPG440B	NGC 5775	12.24(s)		1681	21.2
KPG455A	NGC 5857	13.86(a)	38.4	4682	21.6
KPG455B	NGC 5859	13.27(a)		4764	41.7

(a) Total (asymptotic) magnitude in the B system, derived by extrapolation from photoelectric aperture-magnitude data.
(s) Total asymptotic magnitude in the B system, derived by extrapolation from (surface) photometry with photoelectric zero point.
(p) Photographic magnitude reduced to the $B_{\rm T}$ system.

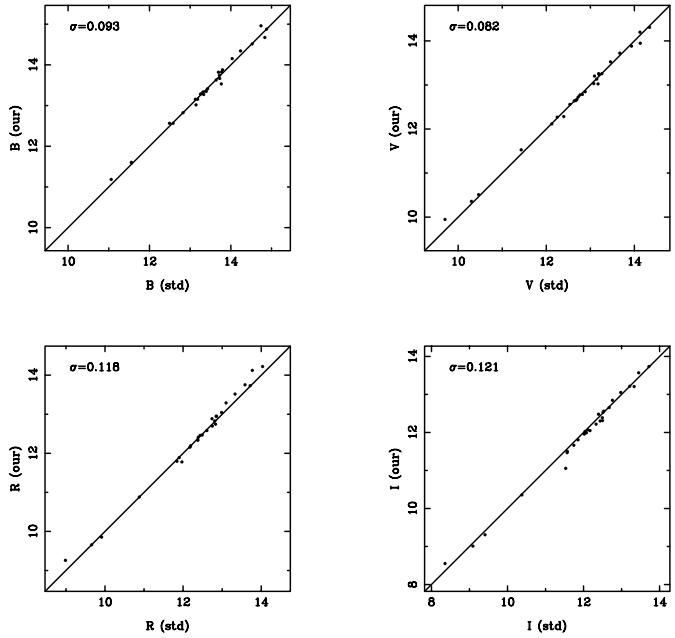

Fig. 1. Comparison between our estimated magnitudes and those from Chevalier & Ilovaisky (1991) for 29 standard stars in common.

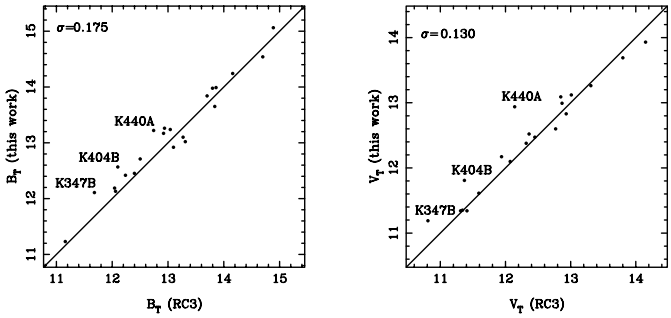

Fig. 2. Comparison between our total B and V magnitudes and total magnitudes from RC3 Catalogue.

The estimated total magnitudes in this work were compared against other external estimations reported in the literature. This has been done for: 1) the standard stars and 2) those paired galaxies in common with other works.

3.2. Standard stars

For the standard stars, a comparison of our CCD magnitudes against those reported in Chevalier & Ilovaisky (1991) for 29 stars in common, are shown in Fig. 1.

Figure 1 shows no significant deviations between our CCD magnitudes and the standard star magnitudes. According to these results, a $\sigma \sim 0.13$, or a similar value, could be expected as the typical error for our magnitude estimations in paired galaxies. This is in agreement with our error estimations.

3.3. Paired galaxies

We begin with a comparison in Fig. 2 of our total magnitudes in B and V bands and those reported in the RC3 Catalogue (de Vaucouleurs et al. 1991).

We find that, except for three galaxies (KPG347B, KPG404B and KPG440A) the agreement with our measures is reasonably good. Rms values from our comparisons are 0.17 and 0.13 mag in B and V bands respectively. However, as noted in Table 3 KPG347 and KPG404 involve two overlapping pairs (CP) where our iterative magnitude estimation procedure could produce some error. In addition, the associated errors in B and V magnitudes reported in RC3 are 0.1 mag for KPG347B and KPG440A and 0.2 mag for KPG404B.

It is important to note that a high fraction of the RC3 data available for our pairs comes from Zwicky photographic magnitudes that were transformed to the $B_{\rm T}$ system ((p) in Table 2). The possibility of systematic errors in the Zwicky magnitudes has been discussed by numerous authors (cf. Haynes & Giovanelli 1984). Although these and other authors present recursion relations to convert Zwicky magnitudes to those of other systems, most notably to the photographic magnitudes in the Holmberg system (1958), or to the $B_{\rm T}$ system (de Vaucouleurs et al. 1991), it has been shown that these recursion relations are probably unsatisfactory for magnitudes fainter than 14.0. For this reason, in Fig. 2 we take into account only the

Table 3. Magnitudes and colour indices.

KPG	B	V	R	I	$B-V$	$B-I$	$B^0_{\rm T}$	$(B-V)^0_{\rm T}$	Notes
KPG64A	13.70	12.92	12.37	11.70	0.78	2.00	13.32	0.66	
KPG64B	15.17	14.21	13.66	12.98	0.96	2.18	14.44	0.75	
KPG68A	13.56	12.82	12.19	11.51	0.73	2.05	13.02	0.58	CP
KPG68B	14.73	13.98	13.31	12.65	0.75	2.08	14.07	0.58	CP
KPG75A	14.62	13.68	13.19	12.18	0.95	2.44	14.07	0.80	
KPG75B	15.36	14.49	13.99	12.97	0.87	2.39	14.50	0.65	
KPG88A	15.06	13.69	12.90	12.17	1.37	2.89	14.13	1.15	
KPG88B	16.12	14.85	14.11	13.44	1.27	2.68	15.21	1.05	
KPG98A	15.62	15.34	14.08	13.28	0.28	2.34	14.76	0.10	
KPG98B	15.51	14.22	13.03	12.07	1.29	3.44	14.89	1.12	
KPG102A	15.68	15.18	14.84	13.87	0.51	1.81	14.98	0.29	
KPG102B	15.06	14.57	14.22	13.42	0.49	1.64	14.41	0.29	
KPG103A	16.27	15.48	14.99	14.18	0.79	2.10	15.66	0.61	
KPG103B	15.12	14.47	14.11	13.42	0.64	1.69	14.62	0.47	
KPG108A	15.17	13.95	13.49	12.55	1.22	2.62	14.31	1.01	
KPG108B	14.35	13.17	12.67	11.76	1.17	2.59	13.45	0.95	
KPG112A	13.24	12.41	11.85	11.19	0.83	2.05	12.33	0.60	CP
KPG112B	13.47	12.63	12.05	11.35	0.84	2.12	12.85	0.68	CP
KPG112s	12.55	11.78	11.20	10.52	0.77	2.03			
KPG125A	13.65	12.88	12.21	11.39	0.77	2.26	13.16	0.63	
KPG125B	12.92	12.15	11.56	10.81	0.77	2.11	12.42	0.63	
KPG136A	14.98	14.29	13.72	13.31	0.69	1.67	14.73	0.58	
KPG136B	15.21	14.34	13.73	13.24	0.87	1.97	14.87	0.75	
KPG141A	15.21	13.96	13.40	12.65	1.25	2.56	14.49	1.06	
KPG141B	14.97	13.92	13.50	12.67	1.05	2.30	14.62	0.95	
KPG150A	14.24	13.26	12.46	11.90	0.98	2.34	13.84	0.86	BS
KPG150B	13.28	12.23	11.57	10.85	1.05	2.43	12.80	0.95	BS
KPG151A	15.40	14.17	13.42	12.77	1.22	2.63	14.32	0.93	CP
KPG151B	15.07	13.87	13.13	12.53	1.20	2.53	14.60	1.05	CP
KPG151s	14.67	13.33	12.55	11.94	1.34	2.73			
KPG156A	13.02	12.60	12.11	11.71	0.42	1.31	12.61	0.30	CP
KPG156B	14.54	13.93	13.42	12.95	0.61	1.59	14.26	0.52	CP
KPG159A	16.39	15.89	15.39	15.45	0.50	0.94	15.90	0.36	
KPG159B	14.61	13.88	13.34	12.95	0.73	1.66	14.16	0.60	
KPG160A	13.98	13.09	12.58	11.74	0.89	2.23	13.80	0.83	
KPG160B	15.44	14.57	14.07	13.23	0.87	2.22	14.83	0.71	
KPG168A	12.80	11.82	11.21	10.68	0.99	2.12	12.29	0.86	CP
KPG168B	15.16	14.23	13.73	13.25	0.93	1.91	14.49	0.77	CP
KPG195A	13.24	12.38	11.81	11.20	0.87	2.04	12.87	0.77	
KPG195B	14.42	13.71	13.28	12.78	0.71	1.64	13.88	0.58	
KPG211A	13.68	12.69	12.01	11.43	0.99	2.25	13.45	0.91	
KPG211B	15.75	14.70	13.99	13.39	1.05	2.36	15.05	0.87	
KPG216A									BS
KPG216B	13.28	12.70	12.37	11.67	0.58	1.62	12.88	0.36	BS
KPG249A	12.45	12.10	11.67	11.42	0.35	1.03	12.26	0.30	CP
KPG249B	12.93	12.50	12.01	11.68	0.43	1.24	12.51	0.32	CP
KPG249s	11.89	11.49	11.03	10.75	0.40	1.14			
KPG295A	13.45	12.59	11.97	11.42	0.86	2.03	13.23	0.79	CP
KPG295B	13.30	12.50	11.92	11.34	0.80	1.97	12.86	0.69	CP
KPG302A	11.23	10.67	10.28	9.64	0.56	1.59	11.03	0.51	
KPG302B	14.05	13.57	13.18	12.56	0.46	1.47	13.90	0.42	
KPG313A	13.17	12.52	12.10	11.87	0.64	1.30	13.09	0.62	
KPG313B	13.26	12.17	11.39	10.68	1.09	2.57	12.97	1.02	
KPG332A	12.19	11.35	10.97	10.14	0.84	2.05	11.91	0.77	
KPG332B	12.71	11.61	11.11	10.09	1.10	2.62	12.04	0.94	
KPG347A	12.13	11.34	10.85	10.26	0.79	1.87	11.97	0.74	CP
KPG347B	12.11	11.19	10.61	9.96	0.92	2.15	11.80	0.83	CP
KPG347s	11.40	10.52	9.96	9.39	0.89	2.02			
KPG389A	13.69	12.99	12.37	12.15	0.71	1.55	13.40	0.61	CP

Table 3. continued.

KPG	B	V	R	I	$B-V$	$B-I$	B^0_T	$(B-V)^0_T$	
KPG389B	13.67	12.83	12.23	11.62	0.84	2.06	13.47	0.76	CP
KPG396A	14.78	14.26	13.84	13.17	0.52	1.61	14.18	0.35	
KPG396B	14.06	13.65	13.28	12.48	0.41	1.57	13.99	0.36	
KPG404A	13.84	13.12	12.60	12.08	0.72	1.76	13.61	0.65	CP
KPG404B	12.57	11.81	11.26	10.63	0.76	1.93	12.33	0.68	CP
KPG426A	14.77	13.78	13.14	12.57	0.99	2.20	14.46	0.88	
KPG426B	15.01	14.11	13.50	13.02	0.90	1.99	14.84	0.82	
KPG440A	13.22	12.94	12.63	12.81	0.28	0.41	13.01	0.22	
KPG440B	12.42	11.34	10.87	9.90	1.08	2.52	11.79	0.92	
KPG455A	13.99	13.11	12.61	11.80	0.88	2.19	13.66	0.78	
KPG455B	13.10	12.47	12.02	11.17	0.63	1.93	12.61	0.50	

CP = Pair apparently in Contact.
BS = Bright Star nearby in the Field.

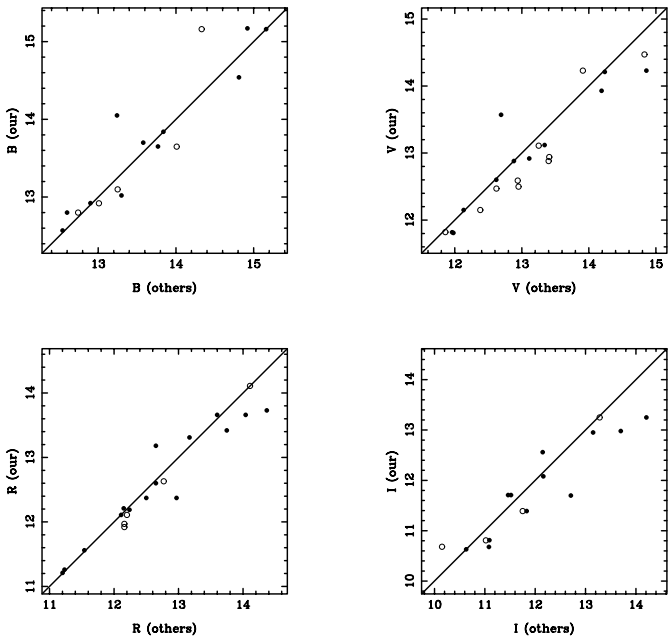

Fig. 3. Comparison between our CCD data and available CCD data from various authors for (S+S) galaxies.

total (asymptotic) magnitudes in RC3 derived by extrapolation either from photoelectric aperture-magnitude data ((a) in Table 2) or from surface photometry with photoelectric zero point ((s) in Table 2).

In relation to this comparison, Reshetnikov (1993) reports that the total magnitudes for interacting galaxies in RC3 obtained by means of photographic photometry are ∼0.2−0.3 brighter compared to magnitudes from surface photometry with photoelectric zero point or by extrapolating the photoelectric data.

The next step involves comparison of our CCD magnitudes with other CCD measures in the four colour bands. Figure 3 shows the comparison with filled symbols denoting CCD measurements in the Cousins system, primarily from Han (1992); Reshetnikov (1993); and Laurikainen et al. (1998). Open symbols denote CCD measurements in the Johnson system, mainly Godwin et al. (1977); Doroshenko & Terebizh (1979); de Vaucouleurs & Longo (1988) and Márquez & Moles (1996). Metcalfe et al. (1998) reports B and V band photometry in the Landolt system while R and I are in the Cousins system. Giovanelli et al. (1997) report I-band data from a combination of sources. No attempt has been made to transform from any of the above photometric systems to Cousins system.

Notice that in Fig. 3 there seems to be no clear systematic tendency between the compared data, in spite of the small number of galaxies in common. The sigma values obtained through a comparison (only) in the Cousins systems are 0.25, 0.25, 0.20 and 0.30 in B, V, R and I respectively. However, it is fair to mention that this is not a straightforward comparison, since we are also comparing both intrinsic and extrinsic differences involved in each photometric system as well as differences in the reduction procedures, that are more easily detected at fainter magnitudes.

Finally, for most paired galaxies, more than one long exposure per filter is available. Thus we evaluate in addition, the internal accuracy of our photometry by comparing the total magnitudes derived from the individual exposures. We find rms differences between individual measurements of $\delta(B) \sim 0.06$, $\delta(V) \sim 0.06$, $\delta(R) \sim 0.05$ and $\delta(I) \sim 0.05$. Additionally, by estimating total magnitudes for all galaxies before and after sky subtraction, typical values $\delta(B) \sim 0.06$, $\delta(V) \sim 0.07$, $\delta(R) \sim 0.06$ and $\delta(I) \sim 0.07$ are obtained. In the Appendix, we report additional estimations of magnitudes at three concentric circular apertures for all the paired galaxies in this study.

4. Discussion

4.1. Integrated magnitudes and colours

The estimated magnitudes and colours of the galaxies in the sample are presented in Table 3. Entries are as follows: Col. (1) gives the identification in Karachentsev Catalogue, Cols. (2) to (5) give the observed total integrated magnitudes in B, V, R and I bands, Cols. (6) and (7) give the observed $(B-V)$ and $(B-I)$ colour

indices. Finally Cols. (8) and (9) give the total corrected $B^0_{\rm T}$ magnitude and $(B-V)^0_{\rm T}$ colour index in the RC3 system. LogR_{25} and the galactic absorption A_B were taken from RC3 Catalogue and Burstein & Heiles (1982), respectively. As stated above, total typical uncertainties in our photometry are 0.15, 0.14, 0.15 and 0.14 for B, V, R and I bands.

Magnitude and colour corrections were not applied for a few small galaxies (blank spaces in Table) in the neighborhood of our pairs, due to a lack of reliable information. Our observations span a range (11, 15.9) and (0.3, 1.1) mag in $B^0_{\rm T}$ and $(B-V)^0_{\rm T}$, respectively. The observed $(B-V)$ range is comparable (by judging the colour maps scales) to that in a similarly selected sample of pairs in the southern hemisphere by Reduzzi & Rampazzo (1996), although some E/S0 components were included in that sample. Interestingly, our $(B-V)^0_{\rm T}$ range is comparable to the full range found in Larson & Tinsley (1978) in spite of the fact that their interacting sample is biased in favour of strongly peculiar systems from the Arp's catalogue. Similarly, the photoelectric Cousins $UBVRI$ photometry of interacting galaxies by Johansson & Bergvall (1990) shows a comparable range in the observed $(B-V)$ colours, although this sample is biased in favour of disturbed morphology, the presence of bridges and includes a fraction of E/S0 components.

4.2. The Holmberg effect

As a byproduct of his famous photometric survey of nearby galaxies, Holmberg (1958) compared the photographic colours of paired galaxies and found a significant correlation between the colours of pair components. This phenomenon has since been referred to as the "Holmberg effect". Figure 4 shows the correlation between the $(B-V)^0_{\rm T}$ colour index. In a few cases irregular galaxies belonging to pairs have conventionally been considered as spirals. The colour index along the vertical axis refers to the brighter (primary) component and that along the horizontal axis refers to the fainter (secondary) component in each pair. To reinforce the validity of any correlation, other symbols indicate sources of $(B-V)^0_{\rm T}$ data for additional (S+S) Karachentsev pairs from the literature.

The colour correlation between pair components is tight. A correlation coefficient $r \sim 0.77$ with a residual sigma of 0.18 is obtained for our (S+S) data. Additionally, a fitting to all the data in Fig. 4, give a correlation coefficient $r \sim 0.70$ with a residual sigma of 0.18. All the (S+S) pairs with $(B-V)$ either from our observations or from the literature, have a median relative velocity, $\Delta v \sim 45$ km s^{-1} and a median projected separation $\Delta x \sim 29$ kpc. Although the physical explanation of the Holmberg effect is complex, it has been interpreted as reflecting a tendency for similar types of galaxies to form together (morphological concordance), a possible reflection of the role of local environment in determining galaxy morphology, but alternatively, it can presumably also reflect

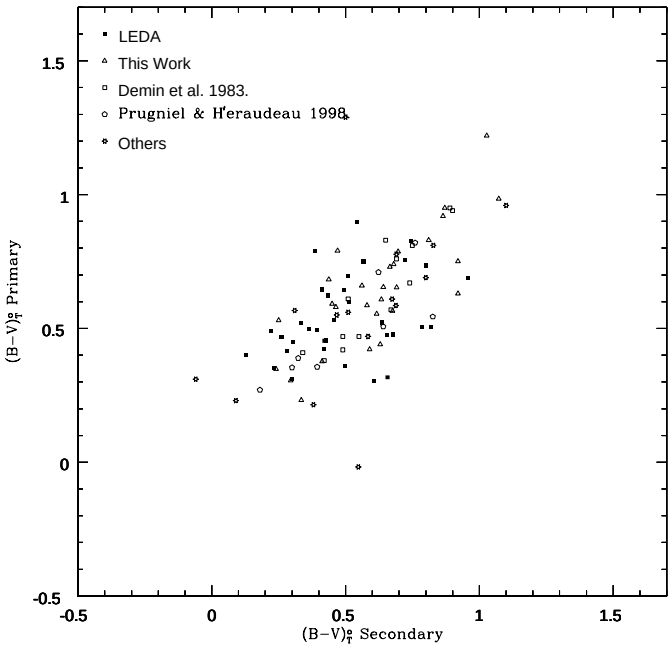

Fig. 4. The Holmberg effect. $(B-V)^0_{\rm T}$ primary versus $(B-V)^0_{\rm T}$ secondary.

mutually induced star formation (Kennicutt et al. 1987) in physical pairs.

4.3. Colours and morphology

To discuss the optical morphology (that could be modified by the presence of bars, spiral arms, rings, etc.) and its relationship to the global photometrical properties, the final results for each pair are presented in the form of a mosaic (Fig. 5) including: 1) mean azimuthally averaged surface brightness and colour profiles, 2) gray scale B-band images, 3) $(B-I)$ colour index maps and 4) B band-filtered images for each pair. In most of the cases, not all the foreground stars in each field have been removed. The images in the lower panels 3) and 4) can be combined to look for morphological features like the presence of bars, rings, the shape of spiral arms, the presence of tidal features and other morphological distortions presumably associated with the interactions. The filtered/enhancing techniques (Sofue 1993 applied in 4), allow the subtraction of the diffuse background in a convenient way to discuss different morphological details.

Karachentsev (1972) identified three basic interaction classes (AT, LI and DI) that describe the pairs which show obvious signs of interaction. AT class identifies pairs with components in a common luminous halo with a symmetric, amorphous or shredded, asymmetric (sh) structure. LI pairs show evidence of tidal bridges (br), tails (ta) or both (br+ta). DI pairs show evidence of structural distortion in one (1) or both (2) components. We add to this sequence NI for the (S+S) pairs with no obvious morphological distortion. The order AT-LI-DI-NI can be regarded as a sequence from strongest to weakest evidence for tidal distortion or, alternatively, most to least dynamically evolved

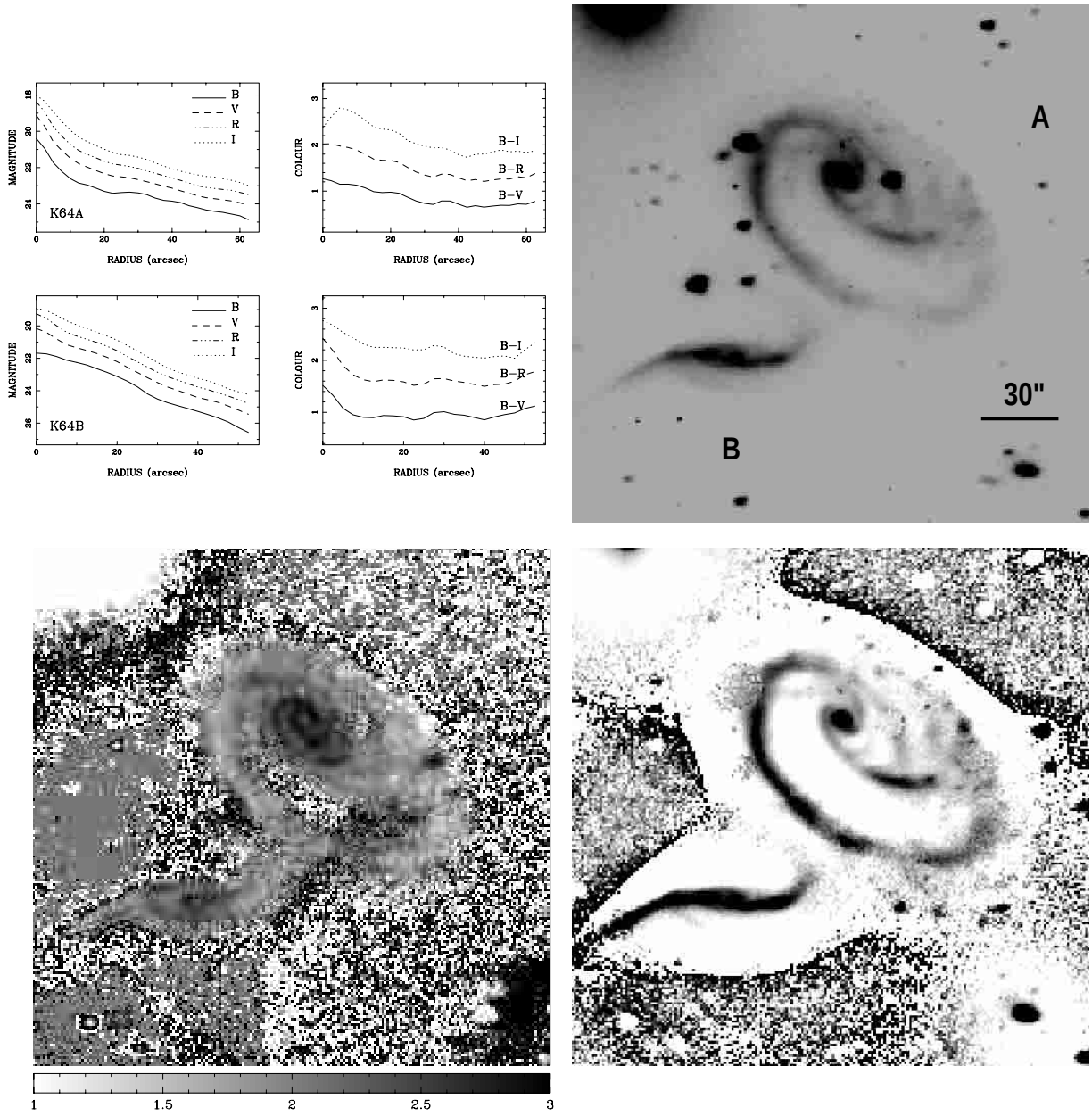

Fig. 5. KPG64 Mosaic. Top left: surface brightness and colour profiles. Top right: B-band image. Bottom left: $B-I$ colour map. Bottom right: enhanced/filtered B-band image. North is to the top and East is to the left.

(interpreting a common envelope as a sign of extensive dynamical evolution in pairs).

Based on our CCD observations, it is now possible to attempt 1) a reclassification of the Hubble morphology from a combination of our colour index $(B-I)$ maps and sharp/filtered B images, 2) a reclassification of the global pair interaction morphology (I/A class hereafter) in the Karachentsev Catalogue and 3) a reclassification of the spiral arm morphology as suggested by Elmegreen & Elmegreen (1982) (hereafter EE class).

It is known that the colours of spiral galaxies are correlated with its morphological type T. Although the colour indices of galaxies belonging to type T will have a large dispersion, the median value declines systematically as T increases along the morphological sequence. Median integrated total $(B-V)$ colours of galaxies according to morphological class are given by Roberts & Haynes (1994). The UGC and the Local Supercluster (LSc) samples in Roberts & Haynes (1994) are rather inhomogeneous in terms of environment, but the interacting objects were excluded from their analysis. We may consider these samples as comparison/reference samples for the following discussion.

4.4. Comments on individual objects

Before proceeding to a discussion of the results shown in tables and figures, we present comments on morphological

details found in individual pairs that may be relevant to our conclusions and look for any relationship to the global photometrical profiles.

KPG64A. The galaxy is classified as SA(s)b pec. Our $(B-I)$ colour map shows two centrally symmetric spiral arms that become bifurcated at the outer parts. The arms are sharp-defined and the B-band sharp/filtered image can show some well-defined knotty structures along them. A bright small nucleus can also be appreciated. We classify this galaxy as Sc pec. The type of arms shown may probably be produced/modified by the interaction as predicted by simulations in Noguchi (1990). The total $(B-V)^0_{\rm T}$ colour is representative of Sab-Sb types. Our EE class is 6.

KPG64B. The galaxy is classified as SB(s)a pec. Our $(B-I)$ colour map shows an apparently inclined galaxy that could be simulating a barred structure in the central region of a lower resolution image. The outer spiral structure resembles an integral sign that could be tidally generated by the interaction, on line with simulations by Noguchi (1990). The sharp/filtered image shows a faint bifurcated structure emanating from the eastern arm. There is also evidence of knotty structure along the arms, but no clear evidence of a bar structure. We classify this galaxy as Sbc. The total $(B-V)^0_{\rm T}$ colour is more representative of S0a-Sa types. We notice that the colour profiles tend to be flat after $15''$. Our EE class is 6. The I/A class for the pair is LI.

KPG68A. This galaxy is overlapping at the southeast with its companion. Our iterative modeling of the light distribution is poor and caution is needed with the total magnitudes and colours for both galaxies. The galaxy is classified as a Scd:. Our sharp/filtered and $B-I$ colour map images shows a bright nucleus plus multiple arms with knotty structure along them. The total $(B-V)^0_{\rm T}$ colour is representative of Sb-Sbc types. Our EE class is 3.

KPG68B. This galaxy is overlapping at the north with its companion. The galaxy is classified as a SBb:. Our sharp/filtered and $B-I$ colour map images shows knotty structure along the arms from either end of a prominent bar. The total $(B-V)^0_{\rm T}$ colour is representative of Sb-Sbc types. The colour profiles in this barred galaxy are flat after $5''$ from its center. The I/A class for the pair is DI. Our EE class is 10.

KPG75A. The galaxy is classified as E?, but our $(B-I)$ and sharp/filtered images show a bright central nucleus from which two opened and diffuse spiral arms emanate. The spiral pattern shows an integral sign (perhaps as a by product of the interaction). We classify this galaxy as Sab. The $(B-V)^0_{\rm T}$ colour is representative of S0a-Sa types.

KPG75B. The galaxy is classified as SB?, and our $(B-I)$ and sharp/filtered images show a bright nucleus and two wrapped adjacent spiral arms that in projection may simulate a bar. We cannot clearly identify a bar structure. The arm at the north appears warped. We classify this galaxy as Sb. The $(B-V)^0_{\rm T}$ colour is representative of Sab-Sb types. The I/A class for the pair is DI. Our EE class is 7.

KPG88A. The galaxy is classified as a SA(s)c and our $(B-I)$ and sharp/filtered images shows a few bright knots along multiple arms that emanate from a bright nucleus. The $(B-V)^0_{\rm T}$ colour is redder than that corresponding to its morphological type. Our estimated $(B-V)$ colour is consistent, however, with that reported by Prugniel & Héraudeau (1998). The colour profiles tend to be flat after $15''$. Our EE class is 12.

KPG88B. The galaxy is classified as a SBcd:. Both our sharp/filtered and $(B-I)$ colour map show a prominent bar and complex arms extending from either end. The $(B-V)^0_{\rm T}$ colour is redder than that corresponding to its morphological type. The I/A class for the pair is DI. Our EE class is 10.

KPG98A. The galaxy is classified as Scd:. Our $(B-I)$ and sharp/filtered images show a bright nucleus plus a perturbed spiral pattern that seems warped in projection. A few knots can be seen along the arms. The $(B-V)^0_{\rm T}$ colour is bluer than that corresponding to its morphological type. We caution the reader about an aparent inconsistency in the results obtained for this pair. Contrary to the observed $(B-V)$ value, the corresponding colour profiles show a tendency to be redder. After repeating the calculations and taking into account our estimated errors in B and V magnitudes, we do not have an explantion for this behaviour. Our EE class is 2.

KPG98B. This galaxy is classified as S?. Our $(B-I)$ and sharp/filtered images show a prominent nucleus plus a faint but defined spiral pattern that simulates an outer pseudo-ring structure. This pattern could be reminiscent of the interaction with its companion. We classify this galaxy as (R)Sa. The $(B-V)^0_{\rm T}$ colour is redder than that corresponding to its morphological type. RC3 Catalogue reports (only) a blue photographic magnitude with an error of 0.2 mag that was transformed to the standard system. However, this value is within 0.2 mag to ours. The I/A class for the pair is DI.

KPG102A. This galaxy is classified as Sa. Our $(B-I)$ and sharp/filtered images show a prominent nuclear structure from which a diffuse wrapped spiral pattern emerges. We classify the galaxy as SBab. The $(B-V)^0_{\rm T}$ colour is bluer than that corresponding to its morphological type.

KPG102B. The galaxy is classified as Sb and our $(B-I)$ and sharp/filtered images show a bright nuclear region plus a beautiful symmetric and sharply-defined spiral pattern that could be caused by the interaction with its companion. We classify the galaxy as Sc. The $(B-V)^0_{\rm T}$ colour is bluer than that corresponding to its morphological type. The $(B-R)$ and $(B-I)$ colour profiles have a tendency to be flat after $10''$. The I/A class for the pair is LI. Our EE class is 11.

KPG103A. The galaxy is classified as Sb. Its small angular size make the visualization of features a difficult task. At our resolution, both the $(B-I)$ and sharp/filtered images shows a peculiar morphology. Keel (1988) has extensively studied this galaxy. The $(B-V)^0_{\rm T}$ colour is representative of a Sab-Sb galaxy. The $(B-V)$ colour profile have a tendency to be flat along the observed radius.

KPG103B. The galaxy is classified as Sa. At our resolution, the $(B-I)$, sharp/filtered and unsharp masking images show a peculiar morphology. The arms appear radially distributed from a prominent bulge. Keel (1988) has extensively studied this galaxy. The $(B-V)^0_{\rm T}$ colour is representative of a Scd-Sd galaxy. The I/A class for the pair is DI.

KPG108A. The galaxy is classified as Sbc. Our $(B-I)$ and sharp/filtered images show a highly inclined galaxy with a bright elongated bulge and a complex dusty structure. It is difficult to find definite signs of perturbation. The $(B-V)^0_{\rm T}$ colour is redder than that corresponding to its morphological type. RC3 Catalogue reports (only) a blue photographic magnitude with an error of 0.2 mag that was transformed to the standard system. However, this value is within 0.2 mag to ours. The $(B-R)$ and $(B-V)$ colour profiles have a tendency to be flat after $25''$.

KPG108B. The galaxy is classified as Sb. Our $(B-I)$ and sharp/filtered images show a highly inclined galaxy with a complex dusty structure. It is difficult to trace signs of perturbation. A small galaxy (north-east) in its neighborhood can be appreciated. The $(B-V)^0_{\rm T}$ colour is redder than that corresponding to its morphological type. RC3 Catalogue reports (only) a blue photographic magnitude with an error of 0.2 mag that was transformed to the standard system. However, this value is within 0.2 mag to ours. The colour profiles have a tendency to be flat after $30''$. The I/A class for the pair is NI.

KPG112A. The galaxy is classified as S0/a. Our sharp/filtered and $B-I$ images show and edge-on galaxy resembling a lenticular or an early-type spiral with a distorted disk. The distorted disk may be representing a tidal tail/counter-tail structure generated by the interaction. We classify this galaxy as Sa. The $(B-V)^0_{\rm T}$ colour is representative of Sab-Sb types. The $(B-V)$ and $(B-R)$ colour profiles tend to be flat after $10''$, while the $(B-I)$ colour profile appear flat all along the observed radius.

KPG112B. The galaxy is classified as S0:. Our sharp/filtered and $B-I$ images show a bright prominent bulge. Two diffuse spiral arms appear wrapped. The arms at the west side are seen, in projection, overlapping at the eastern arm of its companion galaxy. We classify this galaxy as Sa. The $(B-V)^0_{\rm T}$ colour is representative of a Sa galaxy. Our EE class is 12. The I/A class for the pair is LI.

KPG125A. The galaxy is classified as Pec. In spite of its small angular size, our $(B-I)$ and sharp/filtered images show two faint spiral arms emerging from a complex and bright central region. We classify this galaxy as Sab pec. The estimated $(B-V)^0_{\rm T}$ colour is representative of Sab-Sb types. The colour profiles in this galaxy show a tendency to be flat after $5''$.

KPG125B. The galaxy is classified as S pec. However, both our $(B-I)$ and sharp/filtered images show multiple and complex spiral arms with knotty features along them and emanating from a bright nuclear region. We classify this galaxy as Sc pec. The estimated $(B-V)^0_{\rm T}$ colour is representative of Sab-Sb types. The colour profiles show a tendency to be flat after $20''$. The I/A class for the pair is DI. Our EE class is 9.

KPG136A. This galaxy is classified as S?. Our $(B-I)$ and sharp/filtered images show a bright central region from which multiple but diffuse arms appear to emanate. We classify this galaxy as Sbc. The estimated $(B-V)^0_{\rm T}$ colour is representative of Sbc-Sc types. Our EE class is 10.

KPG136B. This galaxy is classified as S?. Our $(B-I)$ and sharp/filtered images show a bright nuclear region surrounded by a tightly wrapped arm-like structure resembling a ring or pseudo-ring. An outer faint feature also resembles a diffuse shell/arc that may be associated with a tidal origin. We classify the galaxy as S(r)ab. The $(B-V)^0_{\rm T}$ colour is representative of a Sa type. The I/A class for the pair is DI. Our EE class is 8.

KPG141A. The galaxy is classified as S?. Our $(B-I)$ and sharp/filtered images show a highly inclined galaxy where a central bulge and a few knots along a thin linear feature (arm seen in projection?) at the north-east can be appreciated. We classify this galaxy as Sbc. The $(B-V)^0_{\rm T}$ colour is redder than that representative of its morphological type. RC3 Catalogue reports (only) a blue photographic magnitude with an error of 0.3 mag that was transformed to the standard system. However, this value is within 1.1 mag of ours.

KPG141B. The galaxy is classified as S?. Our $(B-I)$ and sharp/filtered images show a bright prominent central region and two wrapped but defined arms. We classify this galaxy as Sb. The estimated $(B-V)^0_{\rm T}$ colour is redder than that representative of its morphological type. RC3 Catalogue reports (only) a blue photographic magnitude with an error of 0.3 mag that was transformed to the standard system. However, this value is within 0.3 mag to ours. The I/A class for the pair is DI. Our EE class is 7.

KPG150A. The galaxy is classified as Sa. Our $(B-I)$ and sharp/filtered images show an internal two-arm spiral pattern and a bright nucleus. An outer spiral arm pattern is wrapped and may be resembling, in projection, a pseudo-ring. We classify this galaxy as SA(r)b. The estimated $(B-V)^0_{\rm T}$ colour is representative of S0-S0a types. Our EE class is 7.

KPG150B. The galaxy is classified as SBb. Our $(B-I)$ and sharp/filtered images show a sharply defined bar and multiple knotty arms wrapped enough in the central region to resemble an internal ring. We classify this galaxy as SB(r)c. The colour profiles (in the presence of a bright nearby field star) do not show a tendency to be flat like other barred galaxies in this sample. The estimated $(B-V)^0_{\rm T}$ colour is redder than that representative of its morphological type. Prugniel & Héraudeau (1998) report a blue magnitude in agreement (for a similar aperture) to ours. RC3 Catalogue reports (only) a blue total magnitude with an error of 0.15 mag that was transformed to the standard system. However, this value is within 0.2 mag to ours. The I/A class for the pair is NI. Our EE class is 8.

KPG151A. The galaxy is seen slightly overlapping, in projection, to its companion galaxy at the south-east. The galaxy is classified as Sc. Our $(B-I)$ and sharp/filtered

images show an edge-on galaxy with a clearly defined bulge region. The estimated $(B-V)^0_T$ colour is redder than that corresponding to its morphological type. We could not find a reference in the literature with which to compare magnitudes and colours for this source.

KPG151B. The galaxy is classified as SB?. Our $(B-I)$ and sharp/filtered images show a bright prominent nuclear region and an adjacent elongated feature that resembles a bar. We classify this galaxy as SBb. The $(B-V)^0_T$ colour is redder than that corresponding to its morphological type. RC3 Catalogue reports (only) a blue photographic magnitude with an error of 0.2 mag that was transformed to the standard system. However, this value is within 0.1 mag of ours. The $(B-V)$ colour profile shows a marginal tendency to be flat after 20″. The I/A class for the pair is LI. Our EE class is 8.

KPG156A. The galaxy is classified as SA(r)c pec. Our sharp/filtered and $(B-I)$ images show a bright central nucleus surrounded by two knotty arms forming an inner ring structure. The arms extend far from the center forming: 1) a bridge to its companion and 2) a very long tail. They may be tidally-generated by the interaction. In addition, faint filamentary structures are seen almost tangent to the ring. The estimated $(B-V)^0_T$ colour is definitely bluer than that corresponding to its morphological type. Our EE class is 11.

KPG156B. The galaxy is classified as SB(rs)c pec. However, in our sharp/filtered and $(B-I)$ images no clear ringed structure is noticed. We notice instead, a bright and somehow elongated nuclear region with two diffuse and opened spiral arms resembling a integral sign. We classify this galaxy as SBbc pec. The estimated $(B-V)^0_T$ colour is representative of Sbc-Sc types. The $(B-R)$ and $(B-I)$ colour profiles show a tendency to be flat after 15″. The I/A class for the pair is LI.

KPG159A. The galaxy is classified as Sb. The small angular size of this galaxy does not allow both the sharp/filtered and $(B-I)$ images to show any detailed morphology. The $(B-V)^0_T$ colour is representative of Sm-Im types.

KPG159B. The galaxy is classified as Sb. The sharp/filtered and $(B-I)$ images shows an inclined galaxy with a bright nuclear region and wrapped spiral arms. A faint linear feature crossing the central region resembles a bar. We classify this galaxy as SBb. The $(B-V)^0_T$ colour is representative of Sb-Sbc types. The I/A class for the pair is DI.

KPG160A. The galaxy is classified as SB(s)a. Our $(B-I)$ and sharp/filtered images show a bright outer ring enclosing a bar-like feature. The outer ring is bluer than the adjacent disk. We classify this galaxy as (R')SB(s)a. The $(B-V)^0_T$ colour is representative of S0a-Sa types. The colour profiles show a tendency to be flat after 25″. Our EE class is 8.

KPG160B. The galaxy is classified as SBa. Our $(B-I)$ and sharp/filtered images show a highly inclined system where it is difficult to see the bar and bulge regions. There is knotty structure along the main body of the galaxy. We classify this galaxy as Sb. The $(B-V)^0_T$ colour is representative of Sa-Sab types. If the outer ring in the companion galaxy is regarded as evidence of interaction, the I/A class for the pair is DI, otherwise is NI.

KPG168A. The galaxy is classified as Sa. Our $(B-I)$ and sharp/filtered images show a prominent bulge region and two symmetric spiral arms that simulate a pseudo-ring. In the external parts, the arms are extended and diffuse (resembling an integral sign) forming a bridge to the south-east of its companion galaxy. We classify this galaxy as S(s)b. The $(B-V)^0_T$ colour is more representative of S0-S0a types. The colour profiles show a tendency to be flat from 40″. Our EE class is 6.

KPG168B. The galaxy is classified as Sc. Our $(B-I)$ and sharp/filtered images show an apparently inclined system with a few prominent knots along the main body. Two adjacent diffuse arms are also appreciated. One of them is apparently forming a bridge at the west of its companion galaxy. The $(B-V)^0_T$ colour is more representative of Sa-Sab types. The colour profiles show a tendency to be flat along most of the observed radius. The I/A class for the pair is LI.

KPG195A. The galaxy is classified as SB(s)a pec. The configuration of this pair resembles that of KPG168. Our $(B-I)$ and sharp/filtered images show a prominent bulge and an adjacent linear feature that crosses the central region resembling a bar. From this bar, two spiral arms emerge. These arms are prominent in the central regions and become diffuse and extended (resembling an integral sign) at the external parts. We classify this galaxy as SB(s)b pec. The $(B-V)^0_T$ colour is representative of S0a-Sa types The colour profiles show a marginal tendency to be flat after 40″. Our EE class is 6.

KPG195B. The galaxy is classified as SB(s)m? Our $(B-I)$ and sharp/filtered images show an apparently inclined system with bright condensations along the main body and two adjacent arms that become diffuse at the outskirts. The bar structure is difficult to discerne. We classify this galaxy as Sc. The $(B-V)^0_T$ colour is representative of Sbc-Sc types. The I/A class for the pair is DI.

KPG211A. The galaxy is classified as (R')SAB(rs)ab pec: and our $(B-I)$ and sharp/filtered images seem to confirm this classification. The pattern of spiral arms is complex, tightly wrapped and shows blue colours. This could be a sign of strong perturbation from its companion. The estimated $(B-V)^0_T$ is representative of S0-S0a types. The colour profiles show a tendency to be flat after 30″. Our EE class is 8.

KPG211B. The galaxy is classified as Sb: and our $(B-I)$ and sharp/filtered images show an apparently inclined galaxy with a prominent bulge and two symmetric, diffuse spiral arms. We classify this galaxy as Sa. The $(B-V)^0_T$ colour is representative of S0-S0a types. Our EE class is 7. The I/A class for the pair is DI.

KPG216A. The galaxy has a bright nearby field star that was difficult to subtract in our iterative procedure. The galaxy is classified as SB(s)b pec: Our $(B-I)$ and sharp/filtered images show an elongated central region

resembling a bar structure from which two diffuse spiral arms (integral sign) emerge. Our EE class is 10.

KPG216B. The galaxy is classified as SAB(s)c pec: Our $(B-I)$ and sharp/filtered images show an elongated feature crossing the center and resembling a bar from which two knotty arms emanate. The arm at the west is multiple. We classify this galaxy as SBc pec. The $(B-V)^0_{\rm T}$ colour is representative of Sm-Im types. The colour profiles show structure and a global tendency to be flat after $35''$. The I/A class for the pair is DI. Our EE class is 9.

KPG249A. The pair show an apparent low degree of overlapping. The galaxy is classified as SAB(rs)cd pec. Our sharp/filtered and $(B-I)$ images show two bright condensations in the nuclear region. The arms show a bifurcated spiral pattern and knotty features. The arm at north-east is forming an apparent bridge to its companion galaxy. We classify this galaxy as SABcd pec. The $(B-V)^0_{\rm T}$ colour is more representative of Sm-Im types. The colour profiles show a tendency to be flat after $30''$. Our EE class is 6.

KPG249B. The galaxy is classified as IBm pec. Our sharp/filtered and $(B-I)$ images show some bright condensations along a main elongated body that resembles a bar structure from which two diffuse opened arms emerge. We classify this galaxy as SBm pec. The $(B-V)^0_{\rm T}$ colour is more representative of Sm-Im types. The colour profiles show a tendency to be flat along the observed radius. The I/A class for the pair is LI.

KPG295A. This is a low-degree overlapping pair where both components show remarkably similar morphological features. The galaxy is classified as SAB(rs)a pec and both our $(B-I)$ and sharp/filtered images show a bright nuclear region and a faint adjacent broad feature that may be resembling a bar structure. These features are enclosed by an internal set of blue arms forming an elongated internal ring. In addition, this galaxy also shows an external diffuse and elongated ring. We classify this galaxy as (R')SAB(r)a pec. The $(B-V)^0_{\rm T}$ colour is representative of S0a-Sa types. Our EE class is 8.

KPG295B. The galaxy is classified as SAB(rs)ab pec. Our $(B-I)$ and sharp/filtered images show a galaxy with a prominent nuclear region enclosed by two wrapped arms resembling an inner ring structure. The external arms are bright, blue and wrapped. The $(B-V)^0_{\rm T}$ colour is representative of Sab-Sb types. The I/A class for the pair is DI. Our EE class is 8.

KPG302A. The galaxy is classified as SAB(rs)c:. Our $(B-I)$ and sharp/filtered images show a beautiful spiral structure with knotty blue features all along the arms. We cannot identify signs of a barred structure. We classify this galaxy as Sc. The $(B-V)^0_{\rm T}$ colour is representative of Sc-Scd types. Our EE class is 12.

KPG302B. The galaxy is classified as SB0/a pec. Our $(B-I)$ and sharp/filtered show a prominent and elongated central region that may resemble a bar. Alternatively, we may interpret that as two overlapping bright central sources forming an elongated feature from which two diffuse spiral arms emanate. The arm towards the companion is apparently bifurcated forming an external arc/shell-like feature. We classify this galaxy as SBbc pec. The $(B-V)^0_{\rm T}$ colour is representative of Sd-Sm types. The colour profiles show a tendency to be flat all along its radius. The I/A class for the pair is DI. Our EE class is 6.

KPG313A. The galaxy is classified as SAB(rs)cd. Our $(B-I)$ and sharp/filtered images show a central elongated bar-like feature that is enclosed by a set of arms with apparently differing pitch angles and resembling a broken ring. Blue knotty features are observed along the arms. The $(B-V)^0_{\rm T}$ colour is representative of Sb-Sbc types. The $(B-I)$ colour profile show a tendency to be flat after $40''$. Our EE class is 1.

KPG313B. The galaxy is classified as Sab:sp. Our sharp/filtered and $(B-I)$ images show an inclined galaxy with extended and apparently warped arms. The $(B-V)^0_{\rm T}$ colour is redder than that corresponding to its morphological type. RC3 reports total asymptotic B and V magnitudes with associated errors of 0.15 mag that imply a $(B-V)$ colour in agreement to our observed value. The I/A class for the pair is DI.

KPG332A. The galaxy is classified as SA(rs)c and our $(B-I)$ and sharp/filtered images show a bright nucleus and blue knotty arms. We do not find evidence for an internal ring or s-shaped structure. We classify this galaxy as Sc. The $(B-V)^0_{\rm T}$ colour is representative of Sa type. Our EE class is 3.

KPG332B. The galaxy is classified as Sc: sp and our $(B-I)$ and sharp/filtered images show a spectacular and complex dust lane structure all along the plane of the galaxy. The $(B-V)^0_{\rm T}$ colour is redder than that corresponding to its morphological type. RC3 reports total asymptotic B and V magnitudes with associated errors of 0.1 mag that imply a $(B-V)$ colour in agreement with our observed value. The I/A class for the pair is NI.

KPG347A. The components in this pair show an apparent overlapping but similar morphological types. The galaxy is classified as SA(rs)bc. Our sharp/filtered and $(B-I)$ images show a prominent bulge region and wrapped spiral arms that resemble an inner ring. Blue knotty features are seen along the arms. We classify this galaxy as SA(r)bc. The $(B-V)^0_{\rm T}$ colour is representative of Sa types. Our EE class is 12.

KPG347B. The galaxy is classified as SA(rs)bc. Our sharp/filtered and $(B-I)$ images show an inclined galaxy with a bright nucleus and knotty features along multiple spiral arms. We classify this galaxy as Sc. The estimated $(B-V)^0_{\rm T}$ colour is representative of Sa types. The I/A class for the pair is DI. Our EE class is 3.

KPG389A. The components in this pair have similar morphological features (cf. KPG295) and their arms overlap in the outer region. The galaxy is classified as SAB(s)b pec and our $(B-I)$ and sharp/filtered images show a very definite nucleus and an adjacent small spiral arm enclosed by two external arms. They are knotty and resemble an inner pseudo-ring but become diffuse at large radii. The east arm is seen interpenetrating the west arm of its companion such that an x-like feature is formed.

We classify this galaxy as SA(rs)bpec. The $(B-V)^0_T$ colour is representative of Sb-Sbc types. Our EE class is 6.

KPG389B. The galaxy is classified as SA(s)b: pec and our $(B-I)$ and sharp/filtered images show an elongated nuclear region from which two long and diffuse arms emerge. The west arm appears crossing the east arm of its companion forming an x-shaped feature. We classify this galaxy as SABb pec. The $(B-V)^0_T$ colour is representative of Sa-Sab types. The colour profiles show a tendency to be flat after $20''$. The I/A class for the pair is LI. Our EE class is 7.

KPG396A. The galaxy is classified as SB(s)d: sp. Our $(B-I)$ and sharp/filtered images show an apparently inclined system with an elongated nucleus and a spiral pattern that is difficult to trace. The $(B-V)^0_T$ colour is more representative of Sm-Im types.

KPG396B. The galaxy is classified as SB(s)d. Our $(B-I)$ and sharp/filtered images show a prominent bar structure and a complex, knotty spiral pattern with differing pitch angles. The $(B-V)^0_T$ colour is representative of a Sm-Im types. The colour profiles show structure and a tendency to be flat after $25''$. The I/A class for the pair is DI. Our EE class is 1.

KPG404A. The pair show an apparent low degree of overlapping. The galaxy is classified as SB(s)b pec. Our sharp/filtered and $(B-I)$ images show a prominent nucleus and a faint adjacent linear bar from which two spiral arms (integral sign tidal arms) emanate. The arms are wrapped and simulate an inner ring structure. A third small galaxy can be seen near the end of the western arm (tail). The southern arm is seen forming a bridge to its companion galaxy. We classify this galaxy as SB(r)b pec. The $(B-V)^0_T$ colour is representative of Sab-Sb types. The colour profiles show a tendency to be flat after $25''$. Our EE class is 10.

KPG404B. The galaxy is classified as SA(s)b pec. Our sharp/filtered and $(B-I)$ images show a bright nucleus and apparently strong dust lanes along the arms (see the arm towards the companion galaxy). The $(B-V)^0_T$ colour is representative of Sab-Sb types. The I/A class for the pair is LI. Our EE class is 11.

KPG426A. The galaxy is classified as S?. Our $(B-I)$ and sharp/filtered images show a prominent bulge and barred structure. At either end of the bar, strong condensations and two thin/faint and wrapped arms emanate. There is also indication of a ring enclosing the bar. We classify this galaxy as SB(r)b. The $(B-V)^0_T$ colour is representative of S0-S0a types. The colour profiles show a tendency to be flat after $25''$. Our EE class is 10.

KPG426B. The galaxy is classified as S?. Our $(B-I)$ and sharp/filtered images show a prominent but elongated bulge region and a very faint spiral pattern. An unsharp masking image suggest that an arc-like structure may be present at the western external part. We classify this galaxy as SABb. The $(B-V)^0_T$ colour is representative of S0a-Sa types. The I/A class for the pair is DI. Our EE class is 8.

KPG440A. The galaxy is classified as SAB(rs)d and our $(B-I)$ and sharp/filtered images show a bright central bar and a multiple spiral pattern with knotty structure all along the arms. We classify this galaxy as SBcd. The $(B-V)^0_T$ colour is definitely bluer than that corresponding to its morphological type. Our EE class is 6.

KPG440B. The galaxy is classified as SBc? and our $(B-I)$ and sharp/filtered images show a very complex dust lane structure along the plane of the galaxy, similar to KPG332b. In our images it is difficult to trace the nuclear region, bulge or bar. The $(B-V)^0_T$ colour is representative of E-S0 types. The I/A class for the pair is NI.

KPG455A. The galaxy is classified as SB(s)b and our $(B-I)$ and sharp/filtered images show a bright nuclear region and two faint wrapped spiral arms resembling an inner ring. It is difficult to trace the presence of a bar, although the bulge region is elongated. The spiral pattern becomes diffuse at the outer parts. We classify this galaxy as SA(r)b. The $(B-V)^0_T$ colour is representative of S0a-Sa types.

KPG455B. The galaxy is classified as SB(s)bc but our $(B-I)$ and sharp/filtered images show a bright nucleus from which a spiral pattern emerge. A Blue knotty structure is observed along the arms. At our resolution, we have no clear evidence of a barred structure. We classify this galaxy as SA(s)bc. The $(B-V)^0_T$ colour is representative of Sc-Scd types. The I/A class for the pair is DI. Our EE class is 7.

4.5. Results

Table 4 is a summary of the results found in this work. Column (1) gives the pair catalogued number, Col. (2) gives the Hubble Type as reported in NED, Col. (3) gives the Hubble Type as estimated in this work, Col. (4) gives the Elmegreen (EE) class, Col. (5) gives the revised Karachentsev interaction I/A class, Col. (6) shows when a flat colour profile is present, and finally Col. (7) remarks the presence of Bars, Knots, Rings and Shell structures.

A reclassification of the galaxies in the (S+S) sample was made using our CCD data. The original classifications were made on the low resolution POSS. We revise the Hubble classifications for at least one component in 44% of our pairs (29 galaxies). An appreciable change in Hubble types $\Delta T \geq 2$ was found in 25 galaxies. The bulk of the sample is comprised of (S+S) pairs. Very few galaxies could be classified as irregular, and they may well be severely distorted spirals. If we consider $\Delta T \geq 2$ as a minimum value for morphological discordance in pairs, then half of our pairs show morphological concordance between pair members; 17 pairs (51%) show $\Delta T \sim 1$ and 16 pairs (49%) $\Delta T \geq 2$. This could explain, in part, the strong correlation found between $(B-V)$ colour indices (Holmberg Effect) between members of this sample.

Elmegreen & Elmegreen (1982) developed a 12-division morphological system to classify spiral galaxies according to the regularity of their spiral arm structure.

Table 4. Final results from this study.

Galaxy pair	HUBBLE TYPE(NED)	HUBBLE TYPE(THIS WORK)	EE CLASS	I/A CLASS	PROFILE	NOTES
KPG64A	SA(s)b pec	Sc pec	6	LI		K
KPG64B	SB(s)a pec	Sbc	6		F	K
KPG68A	Scd:		3	DI		K
KPG68B	SBb:		10		F	B, K
KPG75A	E?	Sab		DI		
KPG75B	SB?	Sb	7			
KPG88A	SA(s)c		12	DI	F	K
KPG88B	SBcd:		10			B
KPG98A	Scd:		2	DI	F	K
KPG98B	S?	(R)Sa				R
KPG102A	Sa	SBab		LI		B
KPG102B	Sb	Sc	11		F	
KPG103A	Sc			DI	F	
KPG103B	Sa					
KPG108A	Sbc			NI	F	
KPG108B	Sb				F	
KPG112A	S0/a	Sa		LI	F	
KPG112B	S0:	Sa	12			
KPG125A	Pec	Sab pec		DI	F	
KPG125B	S pec	Sc pec	9		F	K
KPG136A	S?	Sbc	10	DI		
KPG136B	S?	S(r)ab	8			R
KPG141A	S?	Sbc		DI		K
KPG141B	S?	Sb	7			
KPG150A	Sa	S(r)b	7	NI		R
KPG150B	SBb	SB(r)c	8			B, K, R
KPG151A	Sc			LI		
KPG151B	SB?	SBb	8		F	B
KPG156A	SA(r)c pec		11	LI		K, R
KPG156B	SB(rs)c pec	SBbc pec			F	B
KPG159A	Sb			DI		
KPG159B	Sb	SBb				B
KPG160A	SB(s)a	(R')SB(s)a	8	DI	F	B, R
KPG160B	SBa	Sb				K
KPG168A	Sa	S(s)b	6	LI	F	R
KPG168B	Sc				F	K
KPG195A	SB(s)a pec	SB(s)b pec	6	DI	F	B
KPG195B	SB(s)m?	Sc				K
KPG211A	(R')SAB(rs)ab pec:		8	DI	F	B
KPG211B	Sb:	Sa	7			
KPG216A	SB(s)b pec:		10	DI		B
KPG216B	SAB(s)c pec:	SBc pec	9		F	B
KPG249A	SAB(rs)cd pec	SABcd pec	6	LI	F	B, K
KPG249B	IBm pec	SBm pec			F	B, K
KPG295A	SAB(rs)a pec	(R')SAB(r)a pec	8	DI		B, R
KPG295B	SAB(rs)ab pec		8			B, R
KPG302A	SAB(rs)c:	Sc	12	DI		K
KPG302B	SB0/a pec	SBbc pec	6		F	B
KPG313A	SAB(rs)cd		1	DI	F	B, R, K
KPG313B	Sab:sp					
KPG332A	SA(rs)c	Sc	3	NI		K
KPG332B	Sc: sp					
KPG347A	SA(rs)bc		12	DI		K
KPG347B	SA(rs)bc	Sc	3			K
KPG389A	SAB(s)b pec	SA(rs)b pec	6	LI		K
KPG389B	SA(s)b: pec	SABb pec	7		F	B
KPG396A	SB(s)d: sp			DI		B
KPG396B	SB(s)d		1		F	B, K
KPG404A	SB(s)b pec	SB(r)b pec	10	LI	F	B, R

Table 4. continued.

Galaxy pair	HUBBLE TYPE(NED)	HUBBLE TYPE(THIS WORK)	EE CLASS	I/A CLASS	PROFILE	NOTES
KPG404B	SA(s)b pec		11			
KPG426A	S?	SB(r)b	10	DI	F	B, R
KPG426B	S?	SABb	8			B, Sh
KPG440A	SAB(rs)d	SBcd	6	NI		B, K
KPG440B	SBc?					B
KPG455A	SB(s)b	SA(r)b		DI		R
KPG455B	SB(s)bc	SA(s)bc	7			K

F = Flat Colour Profile.
B = Bar.
K = Presence of Knots.
R = Ring.
Sh = Shell.

This spiral arm classification correlates with the presence of density waves as in grand design galaxies. Following that work, we succeeded in classifying 43 spirals. Some of the spirals in the global sample are nearly edge-on, strongly interacting or simply do not fit into the Elmegreen & Elmegreen classes. From 26 barred spirals, 18 are grand design and only 2 are flocculent. From 40 non-barred galaxies, 17 are grand design and 5 are flocculent. Grand design structure seems to be connected with binary galaxies, but strongly for barred than for non-barred galaxies. These results seem to be consistent with those of Elmegreen & Elmegreen (1982). We also have found knotty features in 24 galaxies and have detected rings or pseudo-ring features in 13 galaxies.

Interestingly, a fraction of the spirals have "open arms" that could be interpreted in the framework of the simulations of Noguchi (1990 and references therein). The simulated galaxies have sizes similar to those in our sample. Noguchi's models follow both the stellar and gaseous component evolution in a disc galaxy during the encounter. Briefly speaking, in this scenario of moderate interactions, the bar develops quite soon and it is long-lasting, while the ring develops later and the gas follows the configuration of the ring. Four different phases may be seen: 1) open arms appear (integral sign) after perigalacticon, 2) a bar develops, the arms start to close and the gas start to follow the star configuration, 3) the arms are completely closed around the bar and form a ring; the gas is mainly concentrated in the center and ring, and 4) the ring starts to be disrupted by the dynamics and the overall appearance of the galaxy becomes nearly asymmetric.

As noted above, a fraction of the spirals in our sample (40%/20%) show (bar/ring) features which could be a transient phenomenon of the interaction in Noguchi's models. The bars are always redder while the rings and knots are always bluer compared with the galaxy outskirts. Most of the bridges and tails maintain the colour of the outskirts of the galaxies. The knotty structure along the arms and disks confirms the global nature of the star formation induced by the interactions. From 33 pairs, 20 can be classified according to the I/A class DI, 9 pairs as LI, and 4 pairs as NI. We have not detected any AT class, perhaps as a selection bias from our observing strategy. The sequence AT-LI-DI-NI has been interpreted as a sequence going from strongest to weak for tidal distortion or from most to least dynamically evolved. According to this, our (S+S) pairs are mainly involved in interactions of moderate level.

An interesting correlation has been found between the optical morphology and the global photometric properties in these pairs. From 26 barred galaxies, 15 show a flat behaviour (negligible gradient) in the azimuthally averaged colour profile while from 40 non-barred galaxies, 12 show flat colour profiles. This result may indicate that the bar acts unifying the stellar populations of the bulge and disk, in agreement with a secular evolutionary scenario, and consistent with the results in Gadotti & dos Anjos (2001) and Zaritsky et al. (1994) where barred spiral galaxies have flatter abundance gradients than unbarred spirals.

5. Conclusions

In order to analyze the photometrical signature of gravitational interactions in spiral galaxies, we present results of our $BVRI$ surface photometry for a first set of 33 (S+S) pairs from the Karachentsev (1972) catalogue. We show that our derived parameters are generally in good agreement with those reported in RC3, aperture photometry catalogues and other individual photometric works. In addition, we present multiaperture photometry in order to facilitate further comparisons and contribute to the existing database of aperture photometry. The combination of 2D $(B-I)$ colour maps and sharp/filtered B images appears to be a powerful technique both for morphological classification and for revealing fine structural details most likely related to encounters that are in various early and late stages. There is a tendency of barred galaxies to show grand design morphologies and flat colour profiles. In general our data suggest that our sample is undergoing moderate interactions which appear to be adequate to stimulate a nonaxisymmetric potential that generate a global response as evidenced by the presence of bars, rings, pseudo-rings and knotty structures along the arms and disks of the spiral galaxies in (S+S) pairs.

Acknowledgements. I.P. thanks the staff of the Observatorio Guillermo Haro for the help in the observations and also likes to thank E. Athanassoula for interesting discussions on spiral structure. These discussions were made possible via the ECOS/ANNUIES exchange project M99-U02, for which we are thankful. H.H.T. thanks J. Sulentic for his valuable comments. H.H.T. and I.P. thank the referee Dr. R. Rampazzo for his careful reading of this manuscript. His constructive criticism has helped us to clarify and focus our paper enormously.

Appendix A: Aperture photometry

Since the birth of galaxy photometry (Whitford 1936), the amount of photometric data has increased exponentially (Prugniel 1987). However, this data is inhomogeneous both in quality and format: photographic, photoelectric or more recently, CCD observations. The data are usually presented as centered aperture photometry through circular or elliptical apertures or as photometric profiles. In order to take into account the continuously growing amount of photometric data and at the same time, to make different photometric data reports somehow comparable, we present in Table A.1 our estimations of integrated magnitudes in three concentric circular apertures. Columns (2) and (3) give the logarithm of the aperture radius (in arcmin) for pair component (A) and (B). Columns (4)–(11) give their corresponding magnitudes in B, V, R and I bands, respectively. The small difference in aperture sizes suggest that the contribution of the sky to the errors in the magnitudes is relatively small. Typical uncertainties in the magnitudes are 0.15, 0.14, 0.15 and 0.14 in B, V, R and I bands respectively.

References

Avila-Reese, V., & Firmani, C. 2000, Rev. Mex. A&A, 36, 23
Avila-Reese, V., Firmani, C., & Hernández, X. 1998, ApJ, 505, 37
Baugh, C. M., Cole, S., & Frenk, C. S. 1996, MNRAS, 283, 1361
Bergvall, N., & Johansson, L. 1995, A&AS, 113, 499
Burstein, N., & Heiles, K. 1982, AJ, 87, 1165
Cardelli, J. A., Clayton, G. C., & Mathis, J. S. 1989, ApJ, 345, 245
Chevalier, C., & Ilovaisky, S. A. 1991, A&AS, 90, 225
de Jong, R., & van der Kruit, P. C. 1994, A&AS, 106, 451
de Vaucouleurs, G., de Vaucouleurs, A., Corwin, H. G., et al. 1991, Third Reference Catalogue of Bright Galaxies (New York, Springer-Verlag)
de Vaucouleurs, A., & Longo, G. 1988, Catalogue of visual and infrared photometry of galaxies from 0.5 micrometer to 10 micrometer, University of Texas
Doroshenko, V. T., & Terebizh, V. Y. 1979, Soviet Astron. Lett., 5, 305
Dultzin-Hacyan, D. 1997, Rev. Mex. A&A, 6, 132
Elmegreen, B. G., & Elmegreen, D. M. 1982, MNRAS, 201, 1021
Gadotti, D. A., & dos Anjos, S. 2001, AJ, accepted [astro-ph/0106303]
Giovanelli, R., Haynes, M. P., da Costa L. N., et al. 1997, ApJ, 477, 1
Godwin, J. G., Bucknell, M. J., Dixon, K. L., et al. 1977, The Observatory, 97, 238
Han, M. 1992, ApJS, 81, 35
Haynes, M. P., & Giovanelli, R. 1984, AJ, 89, 758
Hernández-Toledo, H. M., Dultzin-Hacyan, D., González, J. J., & Sulentic, J. 1999, AJ, 118, 108
Holmberg, E. 1958, Lund Medd. Astron. Obs. Ser. II, 136, 1
Jansen, R. A., Franx, M., Fabricant, D., & Caldwell, N. 2000, ApJS, 126, 271
Johansson, L., & Bergvall, N. 1990, A&AS, 86, 167
Junqueira, S., de Mello, D. F., & Infante, L. 1998, A&AS, 129, 69
Karachentsev, I. D. 1972, Catalogue of Isolated Pairs of Galaxies in the Northern Hemisphere, Comm. Spec. Ap. Obs., 7, 1
Kauffmann, G., Charlot, S., & Balogh, M. L. 2001, MNRAS, submitted [astro-ph/0103130]
Kauffmann, G., White, S. D. M., & Guiderdoni, B. 1993, MNRAS, 264, 201
Keel, W. C. 1988, A&AS, 202, 41
Kennicutt, R. C., Roettiger, K. A., Keel, W. C., van der Hulst, J. M., & Hummel, E. 1987, AJ, 93, 1011
Knapen, J. H., & van der Kruit, P. C. 1991, A&A, 248, 57
Lacey, C. G., & Silk, J. 1991, ApJ, 381, 14
Larson, R. B., & Tinsley, B. M. 1978, ApJ, 219, 46
Laurikainen, E., Salo, H., & Aparicio, A. 1998, A&AS, 129, 517
Márquez, I., & Moles, M. 1996, A&AS, 120, 1
Márquez, I., & Moles, M. 1999, A&A, 344, 421
Mayer, L., Governato, F., Colpi, M., et al. 2001, ApJ, 547, L123
Metcalfe, N., Ratcliffe, A., Shanks, T., & Fong, R. 1998, MNRAS, 294, 147
Moore, B., Katz, N., Lake, G., Dressler, A., & Oemler, A. Jr. 1996, Nature, 379, 613
Noguchi, M. 1990, in Paired and Interacting Galaxies: IAU Colloq., 124, 711
Prugniel, Ph. 1987, CDS Bull., 33, 17
Prugniel, Ph., & Héraudeau, Ph. 1998, A&AS, 128, 299
Reduzzi, L., & Rampazzo, R. 1996, A&AS, 116, 515
Reshetnikov, V. P. 1993, A&AS, 99, 257
Roberts, M. S., & Haynes, M. P. 1994, ARA&A, 32, 115
Sofue, Y. 1993, PASP, 105, 308
Stocke, J. T. 1978, AJ, 83, 348
Sulentic, J. W. 1976, ApJS, 32, 171
van Moorsel, G. A. 1982, Ph.D. Thesis, University of Groningen
Whitford, A. E. 1936, ApJ, 83, 424
Xu, C., & Sulentic, J. W. 1991, ApJ, 374, 407
Zaritsky, D., Kennicutt, R. C., & Huchra, J. P. 1994, ApJ, 420, 87